Simulated solar driven photolytic ozonation for the oxidation of aqueous recalcitrant-to-ozone tritosulfuron. Transformation products and toxicity

Rafael R. Solís*, O. Gimeno, F. Javier Rivas, Fernando J. Beltrán

Departamento de Ingeniería Química y Química Física, Universidad de Extremadura. Avda. Elvas s/n 06006 Badajoz (Spain)

Instituto Universitario del Agua, Cambio Climático y Sostenibilidad (IACYS), Universidad de Extremadura, Avda. de la Investigación s/n 06006 Badajoz (Spain)

*Correspondence to Rafael Rodríguez Solís (rrodrig@unex.es; rafarsolis@gmail.com)

ABSTRACT

This work reports the combination of ozone and solar radiation as an advanced oxidation process to remove the herbicide tritosufuron (TSF) in water. Firstly, the recalcitrance of TSF has been assessed, obtaining an ozonation second order rate constant of 5-154 M^{-1} min^{-1} in the range of pH from 5 to 8; while the rate constant with $HO^{\bullet}$ was found to be $(1.8\text{-}3.1)\cdot 10^{9}$ M^{-1} s^{-1}. Secondly, the simultaneous application of simulated solar radiation in between 300-800 nm and ozone resulted positive in the oxidation rate of TSF. Mineralization extent was also higher. Less effective oxidation was achieved after limiting the radiation to the range 360-800 nm or 390-800 nm; also completely inappropriate for mineralization. Thirdly, the detected transformation products (TPs) demonstrated the vulnerability of TSF molecule to be attacked by $HO^{\bullet}$ in the sulfonylurea bridge. The combination of ozone and radiation of 300-800 nm led to the most effective removal of TPs. Finally, after the photolytic ozonation treatment toxicity was also evaluated in terms of phytotoxitity towards the germination and root elongation of *Lactuca Sativa* seeds, and immobilization of *Daphnia Magna*.

Keywords: ozone, simulated solar radiation, tritosulfuron, transformation products, toxicity

1. INTRODUCTION

The development and contribution of pesticides (named as 'Green Revolution') have improved the products quantity and quality of the the food industry. Pesticides with artificial origin have been used systematically after the 1950s decade due to a more demanding and skilled agriculture market. The banned used of the first developed pesticides, highly toxic and persistent and, hence bio-accumulating in the environment, has promoted a stricter legislation and the application of other modern pesticides formulations less aggressive to the environment. Nevertheless, pesticides and their introduction into the environment due to agriculture is considered an important source of organic contaminants of emerging concern (Diamond et al., 2011).

To date, sulfonylurea herbicides have been developed and commercialized worldwide in over 89 countries. Their use is common in all major agronomic crops, land/pasture, forestry and vegetation management (Krämer et al., 2012). In particular, tritosufuron (TSF) is a broad-spectrum post-emergence herbicide developed and commercialized by BASF Company in 2004 under the trade name 'Biathlon®' as a water-soluble formulation. TSF acts mainly through the treated leaves, and not via the soil.

Advanced Oxidation Processes (AOPs) have gained attention in the research community due to their powerful ability to remove organic aqueous pollutants. Intensive scientific exploration of AOPs for water treatment has been conducted. Efficient hydroxyl radical production has been researched, combining UV radiation, hydrogen peroxide, homogeneous catalysis (like Fenton's reagent), ozone, or photocatalysis, among others (Serpone et al., 2017). Regarding to ozone-based AOPs,

much study has been focused on improving pollutant or/and mineralization rates by using UVC ozonation (Kuo, 1999), ozone combined with hydrogen peroxide (peroxone) (Katsoyiannis et al., 2011), homogeneous or heterogeneous catalytic ozonation (Kasprzyk-Hordern et al., 2003), or the recently explored photocatalytic ozonation (Mehrjouei et al., 2015; Xiao et al., 2015, Beltrán and Rey, 2017).

Photocatalytic ozonation emerges as a better performance technology if the results in terms of organic removal, and overall mineralization extent, are analyzed (Xiao et al, 2015). Nevertheless, implementation of heterogeneous catalysts involves the recovering or immobilization of the catalytic solid, and the replace due to inactivation. Additionally, the oxidation by the combination of ozone and UV radiation also covers the oxidation of a wide range of pollutants of diverse reactivity (Oturan and Aaron, 2014). However, the use of UV radiation requires large amounts of electrical energy, raising the cost of depuration with regard to a real application (Miklos et al., 2018). For that reason, this technology has been poorly implemented in real implementation, different for drinking water disinfection (Parson, 2004; Meunier et al., 2006). Nevertheless, UV-based technologies represent a powerful tool to remove organic pollutants, microorganisms and antibiotic resistance genes (Sousa et al., 2017).

So far, few works have focused on the combination of ozone and alternative to UVC (254 nm) radiation. Recently, Somathilake and coworkers (2018) found that UVA photo-assisted ozonation was appropriated for the mineralization of aqueous carbamazepine. In fact, the synergism between ozone and UVA radiation has also been explored with other organics, successfully oxidized and partially mineralized, such as aniline and 4-chlorophenol (Sauleda and Brillas, 2001).

Some works have considered photolytic ozonation with solar or visible radiation for comparison purposes with other more complex technologies, without exploring in detail

the photolytic ozonation system. For example, Rey el al. (2012) achieved comparable effectiveness of photolytic and photocatalytic ozonation of metoprolol. Similar conclusions can be extracted from the photolytic ozonation of DEET with solar or visible radiation (Mena et al., 2017). Other works also support the ability to combine ozone and solar radiation, which might avoid the use of extra hydroxyl radical promotion via the addition of photocatalysts (Márquez et al., 2014; Quiñones et al., 2015). Only few recent research has tested the ozone decomposition rate in the presence of solar simulated radiation, and its application to a mixture of pollutants in simulated effluent of wastewater treatment plant (Chávez et al., 2016) or river water (Solís et al., 2019).

The aims of this work have been: a) the study of photolytic ozonation with simulated solar radiation for the oxidation of the ozone recalcitrant TSF at different wavelength ranges; b) the TSF ozone and hydroxyl radical kinetics; c) the tentative identification of transformation products; and, d) the toxicity evaluation of raw and treated TSF samples with phytotoxicity tests of germination-root length elongation using *Lactuca Sativa* seeds, and immobilization assays of *Daphnia Magna.*

2. EXPERIMENTAL SECTION

2.1. Chemicals

Tritosulfuron (TSF, $C_{13}H_9F_6N_5O_4S$, CAS: 142469-14-5) was analytical standard grade (>99%) and acquired from Sigma-Aldrich® (Germany). Chemicals used for analytical purposes were analytical grade and purchased from Panreac® (Spain). All test and store solutions were prepared with Milli-Q® ultrapure water coming from an Integral 5 system (18.2 MΩ cm). HPLC-grade acetonitrile (Panreac®, Spain) was used for TSF

96 analytical HPLC analysis and MS-grade acetonitrile for qualitative LC-MS-QTOF
97 identification of transformation products.

98 **2.2. Experimental installation and procedure**

99 Solar photolytic ozonation assays were developed in a Suntest CPS+ simulator (1500W,
100 air-cooled Xe arc lamp) in which a 500 mL borosilicate glass spherical reactor was
101 placed, homogeneously maintained under magnetic stirring. The emitted simulated solar
102 radiation was restricted to different ranges by using filters named as Daylight (300-800
103 nm), Storelight (360-800 nm) and Visiblelight (390-800 nm). Ozone was generated in
104 an Anseros COM-AD-01 device and gaseous ozone concentration was monitored in an
105 Anseros-GM apparatus. Figure 1 shows a scheme of the experimental setup and Figure
106 S1 depicts the absorption spectra of the herbicide tritosulfuron and the emission
107 spectrum of the simulated solar radiation with the different filters used.
108 Semi-continuous experiments were carried by feeding ozone and radiation at the same
109 time. The experiments that required darkness were conducted by covering the reactor
110 with aluminum foil in order to maintain similar temperature profiles for comparison
111 purposes. Before starting, the reactor was filled in with 500 mL of TSF solution,
112 dissolved in ultrapure water. At different times samples were extracted from the
113 aqueous solution for analysis. In ozone processes, an inert gas, e.g. nitrogen, was
114 bubbled through samples to remove residual dissolved ozone. The removal of
115 accumulated dissolved ozone was carried out in order to quench the reaction with
116 molecular ozone in all samples, with the exception of those taken for dissolved ozone
117 quantification.

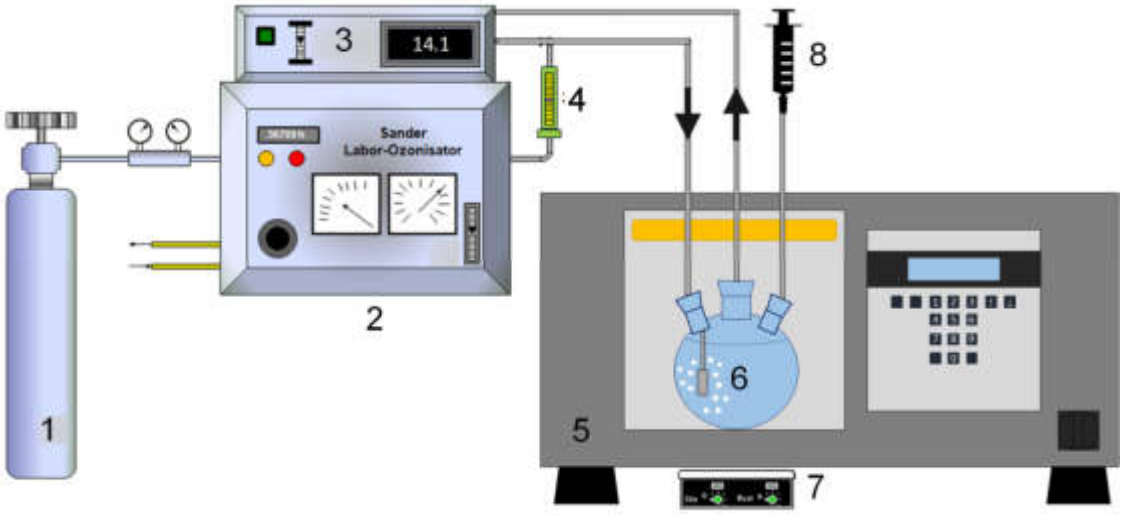

Figure 1. Experimental set-up scheme. 1: Oxygen tank; 2: Ozone Generator; 3: gas-phase ozone analyzer; 4: flowmeter; 5: simulated solar radiation apparatus; 6: borosilicate glass reactor; 7: magnetic stirrer; 8: sampling.

2.3. Aqueous analyses

Aqueous concentration of tritosulfuron was determined by Liquid Chromatography in an HPLC with Diode-Array detection. The apparatus used was a UFLC Shimadzu Prominence LC-AD. A mixture of acetonitrile (A) and water acidified with 0.1% of H_3PO_4 (B) was pumped at a flow rate of 0.5 mL min^{-1}. Core-shell C18 Kinetex® (150x4.6mm, 5µm) was used as stationary phase (thermally maintained at 30ºC) and a 40:60 (v/v A:B) as the mobile phase. Quantification was conducted at 227 nm.

Total Organic Carbon (TOC) and Inorganic Carbon (IC) were determined in a Shimadzu TOC-V_{CSH} analyzer equipped with automatic sample injection.

Inorganic and short-chain organic acids were determined by Ion Cromatography (IC) coupled to a conductivity detector. A Methrom® 881 Compact IC pro equipped with chemical suppression, 863 Compact autosampler and anionic-exchange column (MetroSep A sup 5, 250x4.0 mm, particles of 5µm) thermally maintained at 45 ºC was

136 used. The used mobile phase program consisted of a 0.7 mL min^{-1} gradient of Na_2CO_3
137 aqueous solution from 0.6 mM to 14.6 mM in 50 min.

138 Dissolved ozone concentration in aqueous solution was analyzed by the indigo method
139 (Bader and Hoigné, 1981).
140 The generated hydrogen peroxide was quantified by the colorimetric method based on
141 the cobalt oxidation and complexation with bicarbonate (Masschelein et al., 1977), valid
142 for H_2O_2 concentrations lower than 50 µM. In UVC photolytic decomposition of H_2O_2,
143 used for the hydroxyl radicals' rate constant ($k_{HO\bullet,\ TSF}$) determination, the H_2O_2
144 concentration was spectrophotometrically determined with the titanium (IV) oxysulfate
145 reagent (Eisenberg et al., 1943). A basic 20 Crison® pH-meter equipped with a 50 11T
146 was used for pH measurement.

147 **2.4. Transformation products identification**

148 Transformation products of TSF oxidation via ozonation and photolytic ozonation were
149 analyzed and monitored by HPLC coupled to a Quadrupole Time of Flight (HPLC-
150 QTOF). Experiments with 10 mg L^{-1} of tritosulfuron were carried out for the
151 identification of the main intermediates. In each analysis 5 µL of aqueous sample were
152 injected in an Agilent 1260 HPLC coupled to an Agilent 6520 Accurate Mass QTOF
153 LC/MS. A Zorbax Eclipse Plus C18 column (3.5 µm, 4.6x100 mm) was used for the
154 chromatographic separation at 30ºC. A mixture of pure MilliQ® water (phase A) and
155 acetonitrile (phase B) was pumped at a flow rate of 0.4 mL min^{-1} with the following
156 gradient: A:B with a 90:10 ratio was kept during 2 min and changed to 10:90 in 23 min,
157 keeping thereafter 2 min for equilibration. The QTOF conditions were as follows: ESI(-
158) mode, gas temperature 325ºC, drying gas 10 mL min^{-1}, nebulization 45 psig, Vcap
159 3500 V, fragmentation 100 V, acquisition m/z range 100–1000. MS spectra were
160 processed with Agilent Mass Hunter Qualitative Analysis B.04.00 software assistance.

161 Suspected and potential candidates list based on computational (*in silico*) prediction
162 tools, such as University of Minnesota Pathway Prediction System and PathPred
163 (Bletsou et al., 2015) were also used.

164 **2.5. Toxicity to *Daphnia Magna* & Fitotoxicity to *Lactuca Sativa* assays**

165 Immobilization to *Daphnia Magna* assays was considered for the toxicity analysis
166 before and after the oxidation treatments by using the commercial test kit
167 DAPHTOXKIT F^{TM} (MicroBio Tests Inc., Belgium). The procedure followed for eggs
168 hatch and feeding protocol was in accordance to the OECD guidelines for acute
169 immobilization tests (OECD, 2004). The pH of the extracted samples was adjusted to
170 7±0.1 before analysis. The immobility of the *D. Magna* neonates at 24 h was registered.
171 Phytotoxitiy assays based on the seed germination-root elongation of *Lactuca Sativa*
172 were also used to assess the acute toxicity through the reaction time of ozonation and
173 photolytic ozonation treatments. Briefly, fifteen seeds of *L. Sativa* (*Batavia blonde of*
174 *Paris* lettuce from Vilmorin®, France) were placed in a Petri dish equipped with paper
175 disc and 4 mL of aqueous sample were transferred, moistening the paper disc. Then,
176 Petri dishes were incubated in a germination chamber isolated from light at 22 ºC. After
177 5 days, the root length of each germinated seed (L) was measured. Additionally, a blank
178 control with ultrapure water was done (L_0) in order to calculate the percentage root
179 growth of the tested samples (L/L_0).

180 **3. RESULTS AND DISCUSSION**

181 **3.1. Reactivity and kinetics of tritosulfuron in aqueous ozone systems**

182 The reactivity of TSF with ozone was evaluated by determining the second order rate
183 constant of this reaction, $k_{O3,TSF}$, considering that the slow-kinetic regime develops
184 (Beltrán, 2004). Figure 2 depicts the changes of the normalized concentration of

tritosulfuron and the monitored dissolved ozone concentration profile with time in presence of 5 mM of tertbutanol, as HO• quencher. For the determination of $k_{O3,TSF}$ values, the media of dissolved ozone values after 90 min of ozonation was considered for the calculation, as explained in supplementary material.

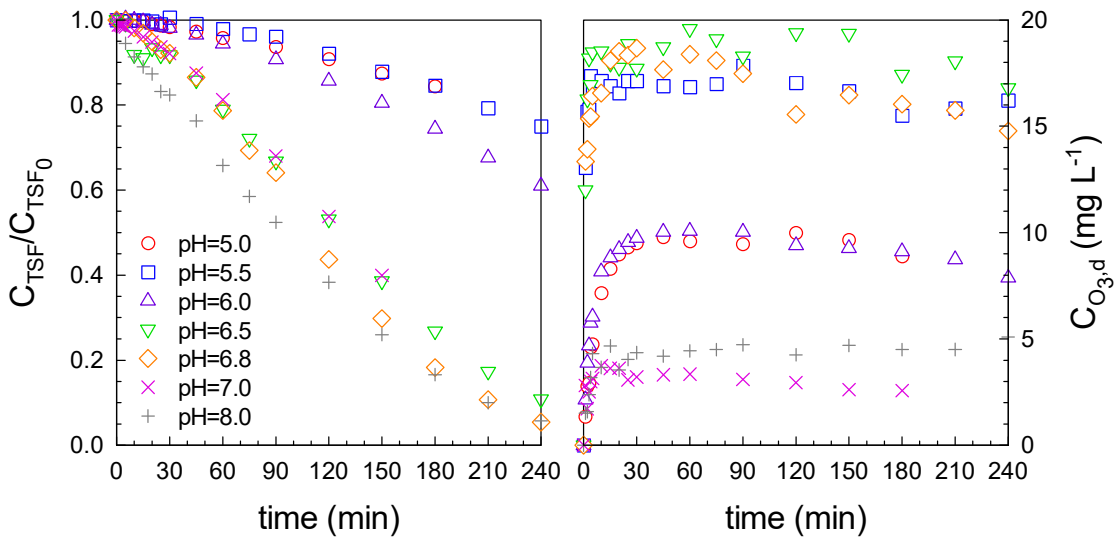

Figure 2. Changes of TSF normalized concentration (left) and dissolved ozone concentration (right) during ozonation in the presence of tert-butanol at different pHs. Experimental conditions: V=500 mL, $C_{t\text{-}BuOH}$=5 mM; C_{H3PO4}=10 mM, Q_{GAS}=33 L h^{-1}, $C_{O3,e}$=75-90 mg L^{-1}, $C_{TSF,0}$=5 mg L^{-1}.

Following the procedure previously described (see also Supplementary information) $k_{O3,TSF}$ values were obtained and the corresponding Hatta number for slow kinetic regime checking (see Table 1). As it is observed, the $k_{O3,TSF}$ calculated values vary from 5 to 150 M^{-1} min^{-1} as pH increases from 5 to 8. The dissociation of the molecule makes the anion species 30 times more reactive than the neutral one.

201 **Table 1.** Second-order rate constant of TSF-ozone reaction at different pHs and

202 corresponding Hatta number (Ha)

pH	$k_{O3,TSF}$ ± error (M^{-1} min^{-1})	R^2	Ha·10^3
5.01	5.5 ± 0.4	0.991	2.08
5.50	4.7 ± 0.3	0.993	1.94
6.01	11 ± 1	0.971	2.96
6.52	35 ± 2	0.993	5.28
6.80	54 ± 5	0.996	7.07
7.00	118 ± 12	0.992	10.8
8.03	154 ± 11	0.990	11.1

203

204 The calculated second-order rate constant was used to extrapolate and calculate the
205 values of the rate constant with the protonated and deprotonated species according to
206 the following equation (Benner et al., 2008):

207 $$k_{O_3,TSF} = \alpha k_{O_3,deprot} + (1-\alpha) k_{O_3,prot} \quad [1]$$

208 where α, the dissociation grade, is defined as:

209 $$\alpha = \frac{1}{1 + \frac{C_{H^+}}{K_a}} = \frac{1}{1 - 10^{pK_a - pH}} \quad [2]$$

210 By using a non-linear least squares regression analysis, experimental data of $k_{O3,TSF}$
211 were fitted to equation [1] to obtain the rate constants of the reactions of ozone with the
212 protonated and deprotonated forms of TSF and the pKa of TSF equilibrium in water.
213 The pKa of the sulfonamide group by itself is 10.1 in solution; however, it is shifted to
214 between 5 and 6.5 depending on the substituents (Kamp et al., 2003). It has to be noted

that the pK_a reported in the bibliography, 4.69 (PPDB, 2018) does not match the one determined here, 6.93. This sort of discrepancy has already been observed in previous work (von Sonntag & von Gunten, 2012) and it was reported as reactive pK_a. According to these authors, such difference is highly related to the reactivity of the functional groups. Thus, the sigmoidal line in Figure 3 depicts the modeled $k_{O3,TSF}$ with pH. The modelled equation [1] gave negligible value for the second-order rate constant of the ozone-TSF protonated form, and 171 M^{-1} min^{-1} for the ozone-TSF dissociated form. The low reactivity towards ozone may be due to the presence of the s-triazine aromatic ring as reported in the literature for similar compounds (Acero et al., 2000; Álvarez et al., 2016) and the deprotonation of the molecule plays an important role during ozone attack.

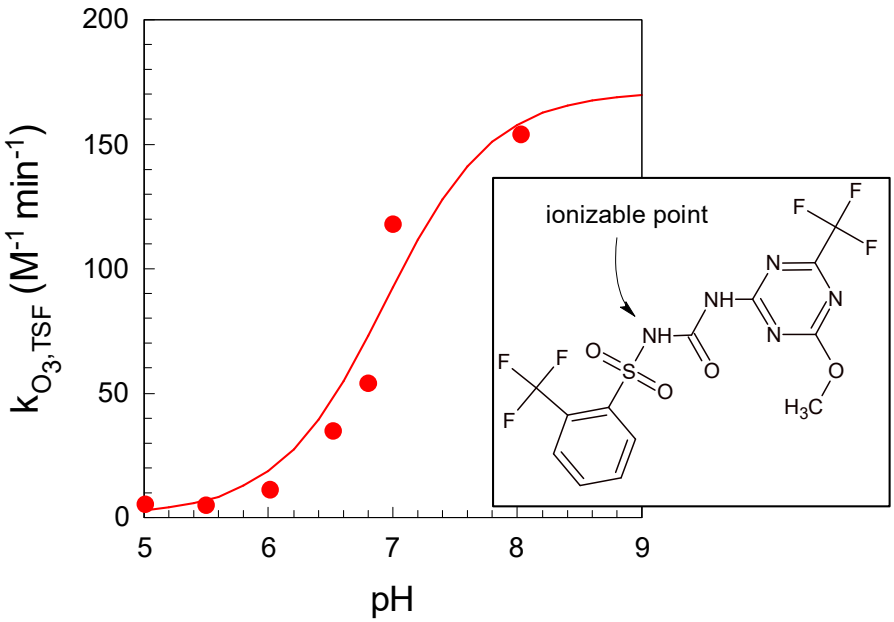

Figure 3. pH dependence of the second-order rate constant of TSF-ozone reaction. Comparison of experimental and calculated values from equation [1] (line)

230 The second order rate constant of TSF-hydroxyl radical reaction was determined with
231 254 nm photolysis in the presence H_2O_2 in excess, (see Supplementary information).
232 TSF abatement in this system for the pHs studied are shown in Figure S3. Least squares
233 analysis of experimental data to fit equation [S8] gave the values of the second-order
234 rate constant in the range of pH=4-9 presented in Table 2. As it can be appreciated,
235 typical rate constant values (average: $2.5 \cdot 10^9$ M^{-1} s^{-1}) were obtained.

236 **Table 2.** Second-order rate constant of TSF-hydroxyl radical reaction at different pHs

pH	($k_{HO\bullet,TSF}$ ± error) 10^{-9} ($M^{-1}s^{-1}$)	R^2
4.01	2.82 ± 0.14	0.998
5.09	3.14 ± 0.09	0.999
6.05	2.43 ± 0.11	0.999
7.03	2.45 ± 0.10	0.999
8.13	1.76 ± 0.09	0.998
9.10	1.27 ± 0.12	0.996

237

238 **3.2. Solar assisted photolytic ozonation**

239 *3.2.1. TSF oxidation*

240 Experiments in the presence of solar radiation where carried out in order to elucidate the
241 effect produced with the simultaneous ozone application. The normalized ozone
242 abatement of TSF and corresponding mineralization (TOC evolution) with time are
243 depicted in Figure 4. For comparison purposes, photolysis, including all the emitting
244 radiation, and single ozonation were experienced. As can be observed, TSF is not
245 photolyzed with Daylight (300-800 nm) radiation. The lack of overlap between TSF
246 radiation absorption spectrum and that of Daylight emission radiation explains this

result (see Figure S1). On the other hand, although this herbicide is highly recalcitrant to ozone, the 90% TSF removal achieved after 2 hours of single ozonation can be explained by the action of hydroxyl radicals. Taking equation [S2] in mind, the experimental conditions followed by ozonation experiment, and the calculated value of $k_{O3,TSF}$, it is possible to simulate the contribution of direct ozonation, by numerically solving the differential equation [S2], i.e. Euler's method (grey line of Figure 4). From the simulated direct ozonation, only a 3% of TSF oxidation could be achieved in 2 hours.

Alternatively, the importance of the hydroxyl radical role can also be examined by calculating the percentage of contribution of the radical pathway ($\eta_{HO\bullet}$) in the process:

$$\eta_{HO\bullet} = 1 - \frac{k_{O_3,TSF} C_{O_3,d}}{k'_{Obs}} \qquad [3]$$

where k'_{Obs} is the apparent pseudo-first order rate constant of TSF oxidation observed in the ozonation process, and $C_{O_3,d}$ the dissolved ozone concentration. Thus, taking into account the time dissolved ozone concentration profile during the reaction, available in Figure 5, and given the fact that k'_{Obs}=1.15 ± 0.04 h^{-1}, more than 99% contribution of hydroxyl radical oxidation is deduced during the ozonation process. Therefore, the assistance of ozone decomposition into hydroxyl radicals via the application of solar radiation seems to be an effective strategy to accelerate the oxidation kinetics of TSF.

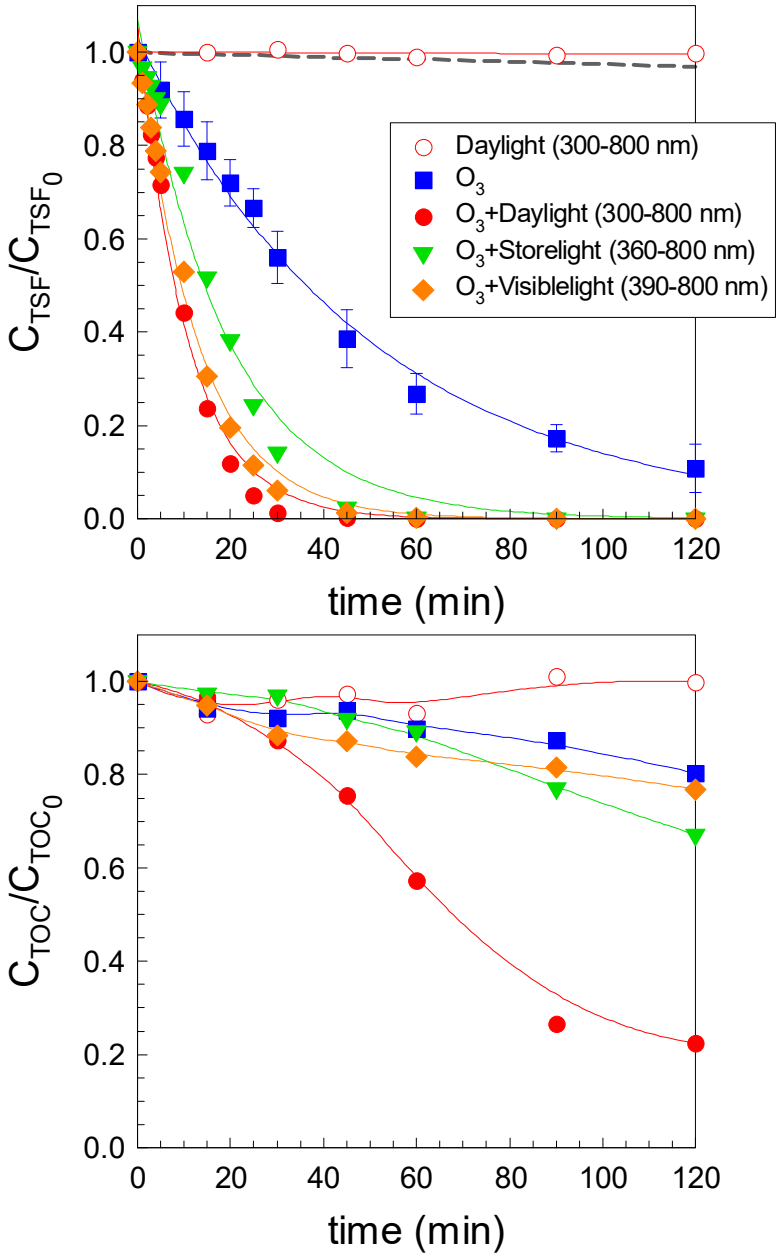

Figure 4. TSF abatement (up) and mineralization evolution (bottom) with time during ozonation and photolytic ozonation. Influence of radiation filters. Experimental conditions: V=500 mL; Q_{GAS}=33 L h^{-1}; $C_{O3,inlet}$=15 mg L^{-1}; $C_{TSF,0}$=10 mg L^{-1}; pH=free. Dashed grey line: direct ozone contribution. Lines in the upper figure: pseudo-first order adjustment.

The simultaneous application of solar radiation and ozone led to a complete abatement of TSF in less than 60 minutes of treatment. If the pseudo-first order rate constant of the process is calculated (k'_{Obs}), just like a mere tool for comparison purpose, the following values are attained: 4.0 ± 0.1 (R^2=0.99), 3.7 ± 0.1 (R^2=0.98), 3.8 ± 0.4 h^{-1} (R^2=0.99) for photolytic ozonation using Daylight (300-800 nm), Storelight (360-800 nm) and Visiblelight (390-800 nm), respectively. This means that the presence of radiation with all the UV portion spectra leads to k' values almost 3.5 higher than in the absence of radiation. Differences between Storelight and Visiblelight were minimal, with approximately 2.8 folded values to single ozonation.

3.2.2. Dissolved ozone and hydrogen peroxide evolution

An analysis of dissolved ozone concentration profiles with time is a useful tool to elucidate the enhanced formation of radicals in the simultaneous presence of radiation and ozone. Figure 5 (left) shows the evolution of dissolved ozone concentration with time in the experiments carried out in the presence and absence of radiation. As can be inferred from Figure 5 (left), when only ozone is applied a stable plateau of 2.1 mg L^{-1} is reached in less than 10 min, under the experimental conditions applied. The addition of Daylight solar radiation has a better decomposition effect, decreasing the value of dissolved ozone concentration to around 0.6 mg L^{-1}. If the less energetic radiation Storelight or Visiblelight is applied, the ozone decomposition is not as remarkable as what was observed with Daylight, reducing the concentration to 1.5 mg L^{-1}. The fact that ozone presents a little absorption of light in the range 300-320 nm (Chávez et al., 2016; Oh et. al., 2016) explains the differences appreciated in the lowest dissolved ozone value reached during the photolytic ozonation with the Daylight filter. The other two filters showed poorer ozone decomposition into radicals due to the almost negligible absorption of ozone.

297 Hydrogen peroxide is a well-known intermediate of aqueous ozonation processes
298 (Sthaehelin et al., 1984). Figure 5 (right) depicts the evolution of the generated
299 hydrogen peroxide concentration through the course of the reaction time. Some
300 interesting results can be appreciated when analyzing this figure. First, the H_2O_2
301 concentration time profile observed during the ozone application reaches a stable value
302 in the range of 14-28 μM. If radiation is simultaneously added, a higher and faster
303 production of H_2O_2 is appreciated, with the exception of visible-range radiation. In
304 particular, the combination of ozone and solar radiation in the range 300-800 nm leads
305 to the highest and faster H_2O_2 formation, reaching a maximum concentration of 52 μM
306 in 30 minutes, followed by almost total H_2O_2 decomposition in 120 min. In the presence
307 of Storelight H_2O_2 reached a slightly lower maximum (50 μM) followed by a lesser
308 decrease if compared to Daylight. Regarding Visiblelight ozonation, a similar profile to
309 that observed during ozonation is registered. In this latter case, a slight decrease in H_2O_2
310 concentration is also observed after 30 minutes of treatment. These results can be
311 explained by analyzing the interaction of radiation and ozone or H_2O_2.

312 Firstly, the higher UV range leads to an enhanced ozone decomposition to form more
313 H_2O_2. Secondly, with higher UV range (especially from $\lambda<360$nm), direct photolysis of
314 H_2O_2 also increases (Chu and Anastasio, 2008; Jacobi et al., 2003) and hence H_2O_2
315 decomposition.

316

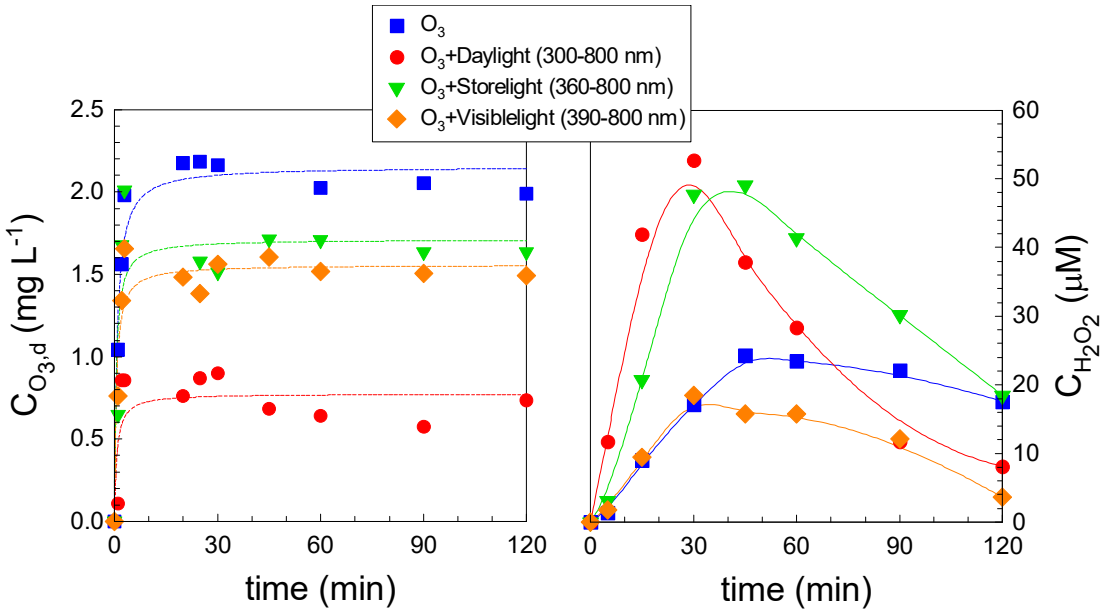

Figure 5. Dissolved ozone (left) and generated hydrogen peroxide (right) evolution during ozonation and photolytic ozonation of TSF. Experimental conditions as shown in Figure 4.

3.2.3. Mineralization & final oxidation products

In terms of mineralization, differences between Daylight and Storelight or visible light were much higher (see Figure 4 bottom). The combination of ozone and solar radiation with all the spectra lead to 80% mineralization in 2 hours. Single ozonation or visible assisted photo-ozonation achieved a poor 20%. The application of Storelight and ozone slightly improved the results of ozonation, achieving 30% of TOC removal.

An analysis of the final oxidation products, i.e. inorganic and organic anions, gives information about the nature of the TOC remaining in these processes. In this sense, Figure 6 shows the evolution of the released inorganic and organic anions during the application of ozone and photolytic ozonation with the different filters. Due to the presence of F, N and S in the TSF molecule, fluoride, nitrate, and sulfate were detected during the process. The most efficient technology was the application of Daylight

radiation and ozone. In this system, a fast fluoride released is appreciated according to the oxidation of the parent TSF molecule in the first fifteen minutes; reaching a final 61% in 120 minutes. In the case of nitrate, all ozone involving systems lead to similar inorganic nitrogen release (~20%), with the exception of photolytic ozonation under Daylight radiation, in which nitrate concentration increased in the last final period (36%). No relevant differences were registered in sulfate profiles, with a maximum 75-79% release

More interesting conclusions can be inferred when comparing the evolution of the formic and oxalic acid concentration profiles. Thus, the application of ozone leads to a low formation of formic and oxalic acids, as expected, due to inefficient mineralization rate of single ozonation. Oxalic acid gradually increased until ~2 mg L^{-1} whereas formic acid presented a maximum of ~1 mg L^{-1} at 45 min with a small decrease. This behavior can be explained by taking in mind the reactivity of these acids towards ozone. It is well known that formic acid is several magnitude orders more reactive to direct ozonation than oxalic acid (Hoigné and Bader, 1983). When radiation is simultaneously applied with ozone, a higher maximum of formic acid is registered with the exception of visible radiation. Daylight+ozone is the most efficient in terms of formic acid production and its oxidation, being completely removed after 90 min. Finally, ozone and ozone+Visiblelight led to similar gradual oxalic acid release whereas Storelight accelerated the gradual generation of this organic acid. However, Daylight+ozone produced the highest oxalic acid production which a maximum in the proximity of ~6 mg L^{-1} at 45 min, and then, it was almost completely oxidized after 2 hours of reaction. In conclusion, the powerful mineralization achieved in photolytic ozonation when applying the UV to the highest extent, that is Daylight (300-800 nm), is intimately related to oxalic and formic acids removal with this system.

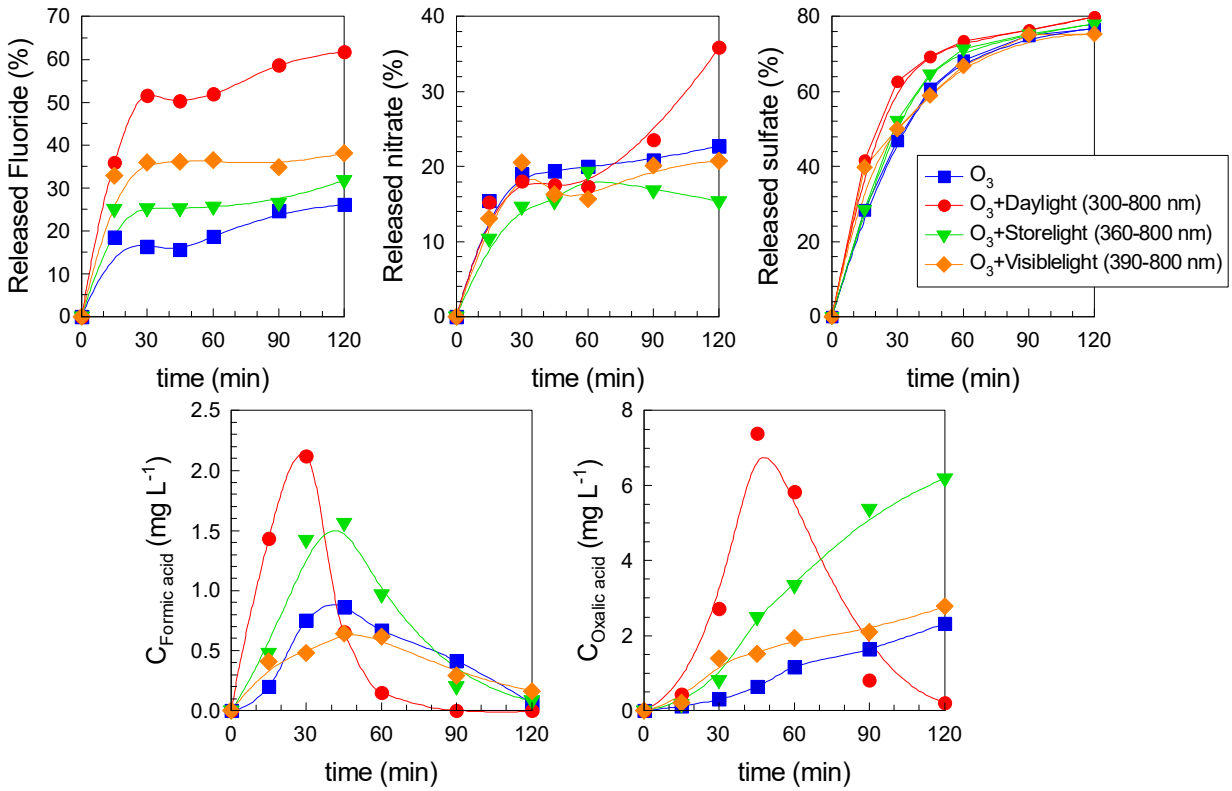

Figure 6. Release of inorganic and organic anions during ozonation and photolytic ozonation of TSF. Experimental conditions as shown in Figure 4.

3.2.4. Transformation products, proposed mechanism and evolution

Degradation pathway was proposed by analyzing the species involved during TSF oxidation by ozone or ozone combined with radiation (Daylight or Visiblelight) by means of LC-QTOF technique. Eight transformation products (TPs) were successfully recognized. Table 3 shows the retention times at which TPs were registered, the formula and structure proposed, the associated error to the experimental mass (in ppm) and the oxidation process in which they were detected. In general, no differences were noticed in the nature of the TPs if ozonation is compared to photolytic ozonation processes. Hydroxyl radical plays, by far, the major role in the TSF oxidation even during single ozonation, the mechanism of oxidation being similar in both technologies. Figure 7 depicts a proposed mechanism of oxidation routes based on the detected TPs.

372 **Table 3.** Proposed Transformation Products (TPs) found by LC-QTOF during
373 ozonation and photolytic ozonation of TSF. Experimental conditions as shown in Figure
374 4

TP & Structure	Retention time (min)	Exact mass $[M-H]^-$ (error, ppm)	Formula	Oxidation process
TP1 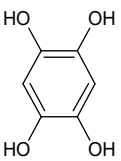	2.35	141.0193 (0.94)	$C_6H_6O_4$	O_3 O_3+Daylight O_3+Visiblelight
TP2 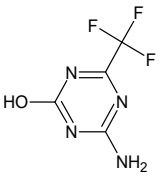	9.75	179.0186 (-13.86)	$C_4H_3F_3N_4O$	O_3 O_3+Daylight O_3+Visiblelight
TP3 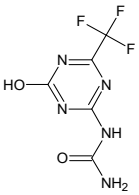	11.42	222.0244 (-12.46)	$C_5H_4F_3N_5O_2$	- O_3+Daylight O_3+ Visiblelight
TP4 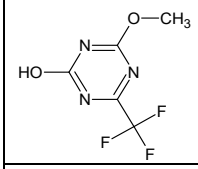	13.69	194.0183 (-13.48)	$C_5H_4F_3N_3O_2$	O_3 O_3+Daylight O_3+ Visiblelight
TP5 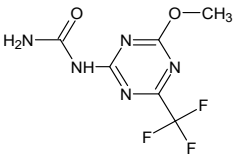	14.95	236.0401 (-13.63)	$C_6H_6F_3N_5O_2$	O_3 O_3+Daylight O_3+ Visiblelight
TP6 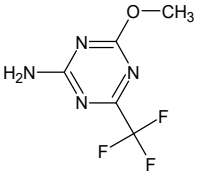	15.34	193.0347 (-14.67)	$C_5H_5F_3N_4O$	O_3 O_3+Daylight O_3+ Visiblelight
TP7	16.14	223.9998	$C_7H_6F_3NO_2S$	O_3

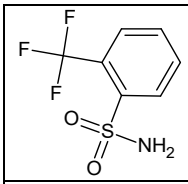		(-11.35)		O_3+Daylight O_3+ Visiblelight
TP8 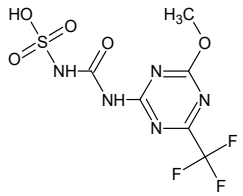	20.36	315.9969 (-11.69)	$C_6H_6F_3N_5O_5S$	O_3 O_3+Daylight O_3+ Visiblelight
TSF 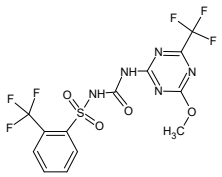	21.47	444.0207 (-0.22)	$C_{13}H_9F_6N_5O_4S$	O_3 O_3+Daylight O_3+ Visiblelight

Sulfonylurea herbicides are characterized by the typical sulfonylated urea bridge. In the particular case of TSF, the sulfonylurea bridge is connected, on one hand, to s-triazine heterocycle with a trifluoromethyl and metoxy groups; and secondly, to an aromatic ring, also with a trifluoromethyl group. From the detected TPs, the sulfonylated urea bridge plays an important role since it seems to be the most vulnerable center to be oxidized (Sarmah & Sabadie, 2002). The cleavage of urea bridge leads to TP7, with a trifluoromethyl and sulfonamide groups. TP7 is considered the main metabolite of TSF degradation because its presence has been reported in aqueous surface samples polluted with TSF (Reemtsma et al., 2013; Kowal et al., 2013) or in soil under aerobic conditions (EFSA, 2015). Further oxidation of TP7 conducts to the loss of these two groups on the aromatic ring, leading to tetrahydroxybenzene (TP1).

TP7 and TP1 where the only two TPs containing the benzene aromatic ring. All the rest intermediates maintained the s-triazine aromatic ring. Although the hydrolytic cleavage of the s-triazine ring has been reported as one of the routes of TSF oxidation (EFSA,

390 2015); the presence of this s-triazine ring in the majority of the detected TPs denotes a
391 high recalcitrance towards hydroxylation. The route of degradation to obtain the s-
392 triazine derived TPs, mainly consisted of the transformation of the parent molecule, i.e.
393 TSF, through the sulfonyl urea bridge that breaks in two possible points. Thus, TP8
394 appears as a consequence of trifluoromethylated benzene aromatic ring loss. The
395 apparition of TP5 can be explained as (1) the loss of a sulfate group of TP8, or (2) by
396 the breakage of the sulfur-nitrogen bond of TSF. A complete oxidation and loss of the
397 metoxy group of TP6 lead to TP3. Alternatively, hydroxylation of the urea bridge of
398 TP5 produces TP6. TP6 shows further oxidation through two possible routes; firstly, by
399 oxidation of the amine group resulting in a hydroxylated derivative, and secondly, by
400 the loss of the metoxy-alkyl chain.

401 All TPs presented the trifluoromethyl substituent, with the exception of TP1. However,
402 the release of fluoride observed by ionic chromatography indicates that other undetected
403 defluorinated organics must be present after these first oxidation steps. The reaction of
404 fluorinated compounds is not favored by hydroxyl radical substitution as happens with
405 other halogens, due to the hampering effect and the strong electron-withdrawing nature
406 of fluorine atoms (Von Sonntag & von Gunten, 2012). The maintenance of $–CF_3$ in the
407 byproducts is commonly appreciated in other oxidation studies of organics similar to
408 TSF (Ellis and Mabury, 2000; Méndez-Arriaga et al., 2011). Little research is available
409 about how fluoride is released. Trifluoromethyl is expected to be transformed into the
410 carboxylic group when attacked by hydroxyl radical, with the subsequent release of
411 fluoride (Lam et al., 2005; Boscá et al., 2001, Ellis and Mabury, 2000). The formation
412 of trifluoracetic acid has also been reported under UVA or solar radiation. The pH and
413 the degree of electron donating-withdrawing of the *ortho* substituent to $–CF_3$ groups
414 define the yield production of fluoride or trifluroacetic acid (Ellis and Mabury, 2000).

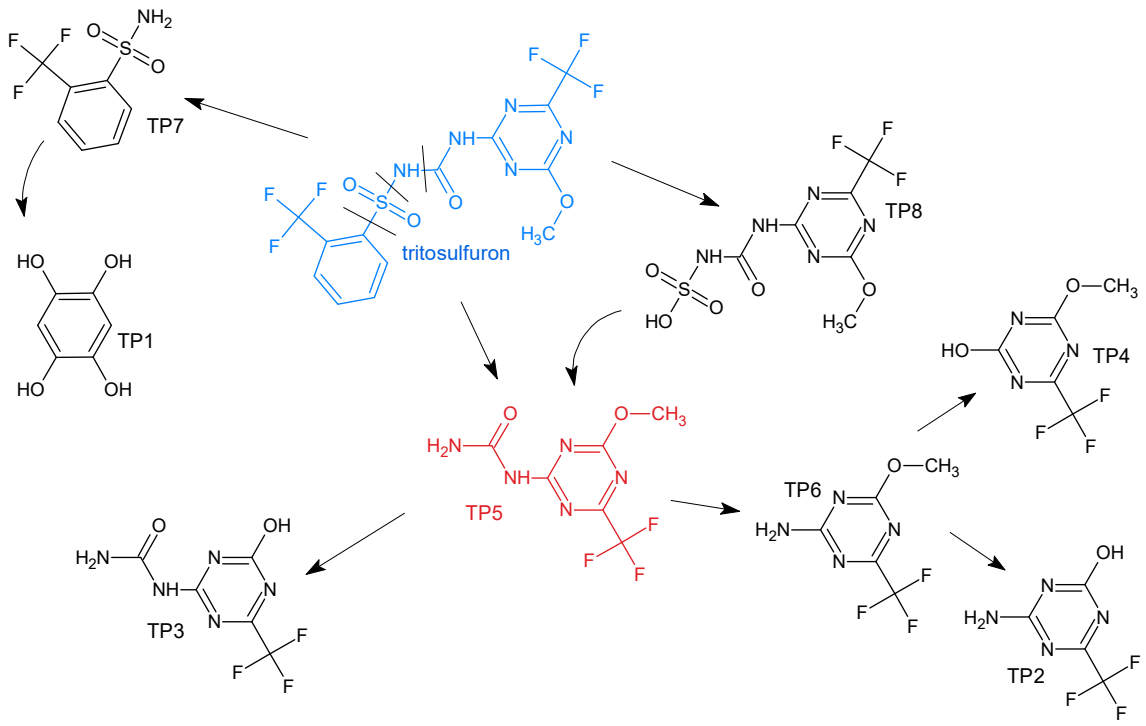

Figure 7. Proposed mechanism of TSF oxidation during ozonation and photolytic ozonation processes based on the detected TPs

The evolution of the tentatively detected TPs through the oxidation time was studied by registering the peak area of the Extracted Ion Chromatograms (EIC). Figure 8 depicts the EICs peak area versus time for ozonation, Visiblelight-photolytic ozonation, and Daylight-photolytic ozonation. Total Ion Chromatograms (TICs) at 30 and 60 min are also presented in Figure S4. Peak areas for all TPs are not proportional to the concentration in the same extent, i.e. intensity of each detected mass strongly depends on operating conditions and easiness to be ionized. Nevertheless, EICs peak areas can be assumed as a tool for comparison of TPs evolution during the oxidation technology. TP1, TP5, and TP8 appear in higher intensities; and they could be considered as the major intermediates. The profile of the rest appears in one less magnitude of intensity.

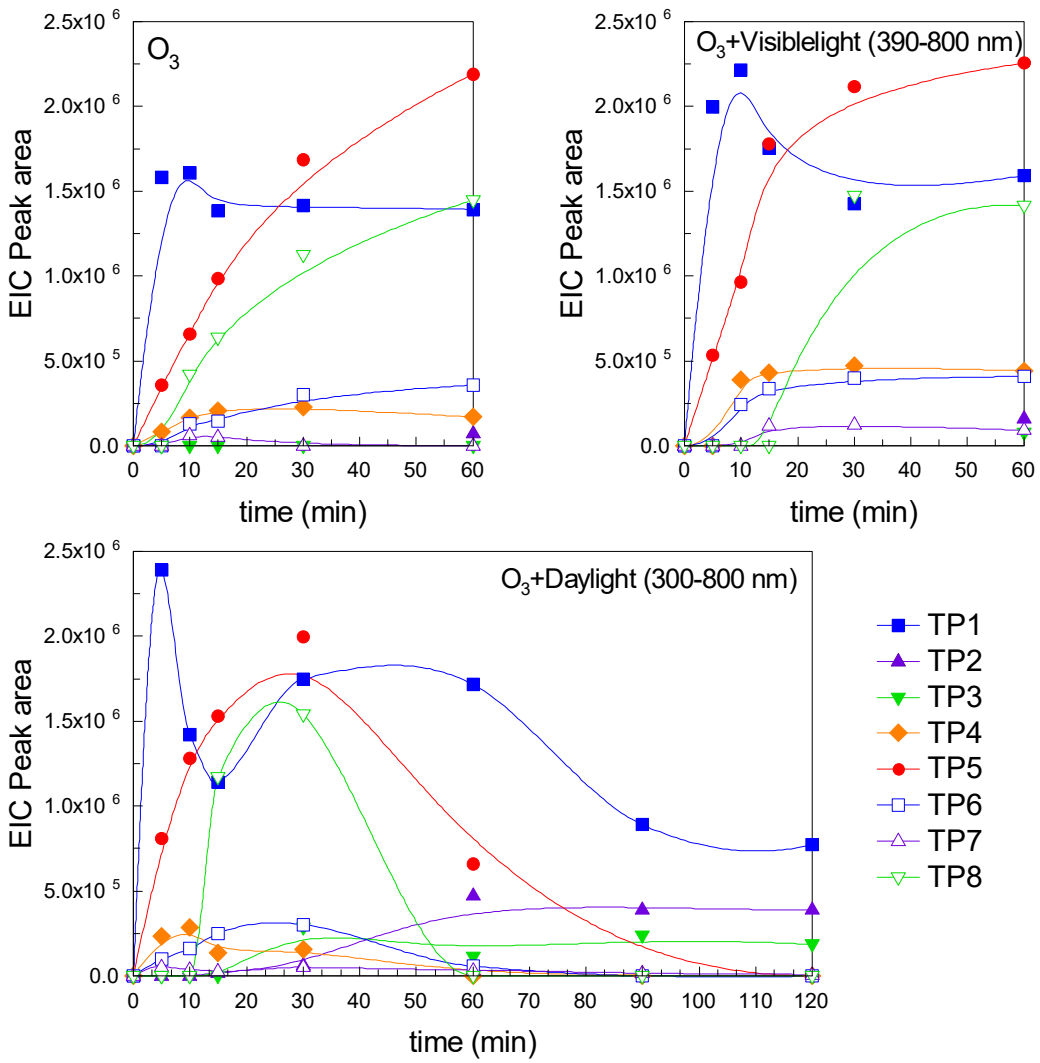

429

430 **Figure 8.** Peak areas evolution of the Extracted Ion Chromatograms (EICs) for the
431 identified Transformation Products (TPs) in the ozonation (top-left) and photolytic
432 ozonation with Daylight (300-800 nm) (down) or Visiblelight (390-800 nm) (top-right)
433 radiation. Experimental conditions as shown in Figure 4.

434 TP1 reached maximum formation after 5-10 min of oxidation, its intensity is higher
435 according to the following order: Daylight photolytic ozonation>Visiblelight photolytic
436 ozonation> ozonation. The release of TP5 and TP8 was also faster when applied
437 O_3+Daylitht radiation, reaching their maxima at 30 min to significantly decrease at 60
438 min. Ozonation and Visible-photolytic ozonation accumulated TP5 and TP8 with

439 reaction time. The higher accumulation of intermediates at 30 min for Daylight+ozone
440 is also observed by comparing the TICs for the three systems (Figure S4). In 30 min,
441 Daylight+ozone leads to a complete removal of the parent compound with a more
442 production of TPs that appear as peaks of higher intensity in the TIC.

443 TP4, TP6, and TP8 are accumulated in the aqueous media for ozonation and
444 Visiblelight-photolytic ozonation, whereas Daylight-photolytic ozonation is capable of
445 removing them completely after 60 min.

446 TP2 appears after further oxidation of TP6. Only Daylight combined with ozone is able
447 to degrade TP6 and launch the formation of TP2. Softer oxidation via O_3 or
448 O_3+Visiblelight radiation seems to be inefficient for the transformation of TP6 which
449 accumulates and impedes the formation of TP2. Similar trends were observed for TP3,
450 generated after oxidation of TP5. As TP5 is oxidized, the formation of TP3 is triggered;
451 this behavior only being observed in Daylight photolytic ozonation.

452 *3.2.5. Phytotoxicity to Lactuca Sativa and immobilization to Daphnia Magna*

453 Toxicity bioassays have positively been used as a reliable tool to evaluate whether
454 effluent detoxification takes place (Rizzo, 2011). This especially applies to those cases
455 where partial oxidation of organic compounds is appreciated. The study of
456 immobilization of *Daphnia Magna* is postulated as the most popular test due to its
457 reproducibility and easy procedure. Moreover, the seed germination of *Lactucca Sativa*
458 assays as target species has been successfully tested to study the changes in toxicity
459 terms during AOPs processes (Andreozzi et al., 2008). In this work, both tests have
460 been considered for the evaluation of the detoxification of TSF. Figure 9 depicts the
461 results obtained.

462 The inhibition growth on other target vegetables has been reported for similar
463 sulfonylureas herbicides (Kotoula-Syka et al., 1993). TSF shows a low-moderate
464 inhibition on the germination-root elongation of *L. Sativa*. As can been appreciated in
465 Figure 9 (A & B), the untreated samples containing 10 mg L^{-1} TSF led to ~50% of
466 inhibition on the lettuce growth. Figure 9A shows how photolytic (Daylight radiation)
467 ozonation process is able to completely remove the phytotoxic character. Thus, seeds
468 reach after the treatment (120 min) a 100% growth length. In contrast, the application of
469 only ozone led to 85% growth length after the same time of treatment. Therefore, after
470 ozonation, a 15% of phytotoxic content remains, likely due to the influence of
471 accumulated intermediates. By comparing ozonation and photolytic ozonation, the
472 addition of Daylight radiation does not only remove phytotoxicity in a higher extent but
473 also leads to a faster evolution of the percentage growth of *L. Sativa*. When radiation is
474 filtered to have a less UV-containing range, ozone+photolysis is less effective to
475 remove phytotoxicity (Figure 9B). The order of effectiveness is
476 Daylight>Storelight>Visiblelight.
477 Ecotoxicity test using the commercial DAPHTOXKIT F magna™ was used to evaluate
478 the toxicitiy of the untreated and treated samples after 120 min (Figure 9C). The
479 untreated sample presented 80% of immobilization of the *daphnis* after 24 hours of
480 exposition. Other sulfonylureas have been reported to be considerably toxic to *D.*
481 *Magna* (Zaltauskaité and Brazaityté, 2013) with over 80% mortality of crustaceans.
482 When applying 120 min of ozonation, less than 50% inhibition is appreciated. If solar
483 radiation is applied in the ozonation process, the toxicity is reduced to only 25% in the
484 best of the cases. This, once again, proves the effectiveness in terms of detoxification of
485 ozone application with the all UV available range in the solar spectrum
486 (ozone+Daylight).

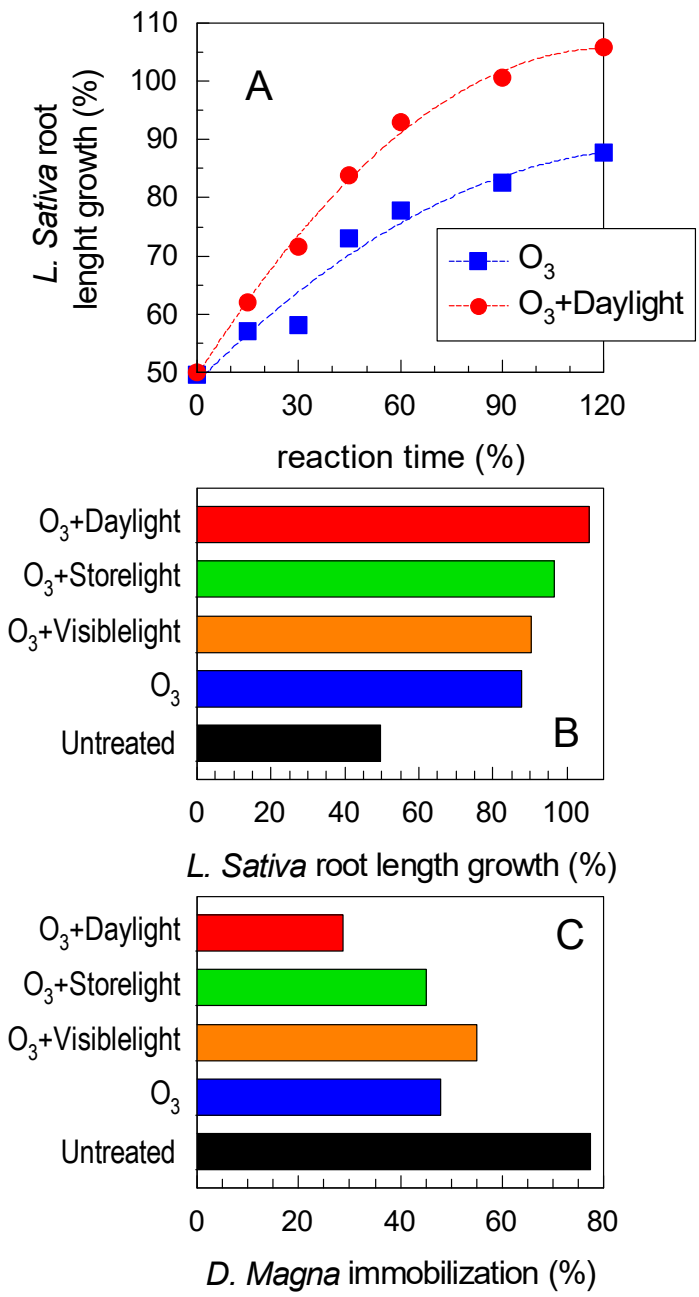

487

488 **Figure 9.** *L. Sativa* root-length growth and *D. Magna* immobilization during the
489 ozonation and photolytic ozonation of TSF. **A:** Root-length growth evolution of
490 ozonation *versus* Daylight photolytic ozonation. **B:** Root-length growth of untreated and
491 120 min treated samples. **C:** *D. Magna* immobilization after 120 min of treatment with
492 24 hours of exposure to the crustaceans. Experimental conditions as shown in Figure 4.

493

4. CONCLUSIONS

From the obtained results the following conclusions were reached:

Application of simulated solar radiation in ozone processes postulates as a promising alternative to enhance the removal rate of oxidation recalcitrant organics, such as TSF. The application of solar radiation (Daylight) and ozone is the most effective process in terms of TSF oxidation. Storelight and vis-photolytic ozonation also improve TSF removal rates if compared to single ozonation. However, in terms of mineralization the role the UV radiation plays results of high importance. Only Daylight+ozone considerably improved the mineralization rate, reaching 80% of TOC oxidation. This behavior is intimately related to the ability of this system to remove refractory organics to ozone final organic acids, like oxalic acid

From the TPs tentatively identified from LC-QTOF technique, the cleavage of TSF in the sulfonyl urea bridge is proposed. The s-triazine aromatic and the–CF_3 groups showed recalcitrance to oxidation, the application of ozone+Daylight being the most effective for degradation as fluoride release confirms.

Finally, from the analysis of toxicity of the treated samples through *L. Sativa* phytotoxicity analyses and *D. Magna* immobilization, a higher detoxification of Daylight-photolytic ozonation process is observed.

Acknowledgements

The authors are grateful to Junta de Extremadura (Project IB16022), co-financed by the European Funds for Regional Development, for economically supporting this work. Moreover, it is also acknowledged the *'Servicio de Análisis Elemental y Molecular (SAEM)'*of '*Servicios de Apoyo a la Investigación de la Universidad de Extremadura (SAIUex)'* for the helping with the intermediate products analyses.

518 **REFERENCES**

519 Acero, J.L., Stemmler, K., von Gunten, U., 2000. Degradation kinetics of atrazine and
520 its degradation products with ozone and OH radicals: a predictive tool for drinking
521 water treatment. Environmental Science & Technology 34 (4), 591-597.

522 Álvarez, P.M., Quiñones, D.H., Terrones, I., Rey, A., Beltrán, F.J., 2016 Insights into
523 the removal of terbuthylazine from aqueous solution by several treatment methods.
524 Water Research 98, 334-343.

525 Andreozzi, R., Canterino, M., Di Somma, I., Lo Giudice, R., Marotta, R., Pinto, G.,
526 Pollio, A., 2008. Effect of combined physico-chemical processes on the phytotoxicity of
527 olive mil wastewaters. Water Research 42 (6-7) 1684-1692.

528 Bader, H., Hoigné, J., 1981. Determination of ozone in water by the indigo method.
529 Water Research 15 (4), 449-456.

530 Beltrán, F.J., 2004. Ozone reaction kinetics for water and wastewater systems. CRC
531 Press, Lewis Publishers, Boca Ratón (Florida).

532 Beltrán, F.J., Rey, A., 2017. Solar or UVA-Visible Photocatalytic Ozonation of Water
533 Contaminants. Molecules, 22(7), 1177-1205.

534 Benner, J., Salhi, E., Ternes, T., von Gunten, U., 2008. Ozonation of reverse osmosis
535 concentrate: kinetics and efficiency of beta blocker oxidation. Water Research 42 (12),
536 3003-3012.

537 Bletsou, A.A., Jeon, J., Hollender, J., Archontaki, E., Thomaidis, N.S., 2015. Targeted
538 and non-targeted liquid chromatography-mass spectrometric workflows for
539 identification of transformation products of emerging pollutants in the aquatic
540 environment. TrAC Trends in Analytical Chemistry 66, 32-44.

541 Boscá, F., Cuquerella, M.C., Marín, M.L., Miranda, M.A., 2001. Photochemisty of 2-
542 hydroxy-4-trifluoromethylbenzoic acid, major metabolite of the photosensitizing
543 platelet antiaggregant drug trifusal. Photochemistry and Photobiology 75 (5), 463-468.

544 Chávez, A.M., Rey, A., Beltrán, F.J., Álvarez, P.M., 2016. Solar photo-ozonation: a
545 novel treatment method for the degradation of water pollutants. Journal of Hazardous
546 Materials 317, 46-43.

547 Chu, L., Anastanio, C., 2005. Formation of hydroxyl radical from the photolysis of
548 frozen hydrogen peroxide. Journal of Physical Chemistry A 109 (28), 6264-6271.

549 Diamond, J.M., Latimer, H.A., Munkittrick, K.R., Thornton, K.W., Bartell, S.M., Kidd,
550 K.A., 2011. Prioritizing contaminants of emerging concern for ecological screening
551 assessments. Environmental Toxicology and Chemistry 30 (11), 2385-2394.

552 European Food Safety Authority (EFSA), 2007. Opinion on the toxicological relevance
553 of the soil and groundwater metabolite TBSA of tritosulfuron in the context of the
554 human risk assessment. The EFSA Journal 621, 1-33.

555 Eisenberg, G.M., 1943. Colorimetric determination of hydrogen peroxide. Ind Eng
556 Chem Anal Ed 15 (5), 327-328.

557 Ellis, D., Mabury, S.A., 2000. The aqueous photolysis of TFM and related
558 trifluoromethylphenols. An alternate source of trifluoroacetic acid in the environment.
559 Environmental Science and Technology 34 (4), 632-637.

560 Hoigné. J., Bader, H., 1983. Rate constant of reactions of ozone with organic and
561 inorganic compounds in water-II: dissociating organic compounds. Water Research 17
562 (2), 185-194.

563 Jacobi, H.W., Kwakye-Awuah, B., Schrems, O., 2004. Photochemical decomposition
564 of hydrogen peroxide (H_2O_2) and formaldehyde (HCHO) in artificial snow. Annals of
565 Glaciology 39, 29-33.

566 Kamp, F., Kizilbash, N., Corkey, B.E., Berggren, P.O., Hamilton, J.A., 2003
567 Sulfonylureas rapidly cross phospholipid bilayer membranes by a fre-diffusion
568 mechanism. Diabetes 52, 2526-2531.

569 Kasprzyk.Hordern, B., Ziolek, M., Naweocki, J., 2003. Catalytic ozonation and methods
570 of enhancing molecular ozone reactions in water treatment. Applied Catalysis B:
571 Environmental 46 (4), 639-669.

572 Katsoyiannis, I.A., Canonica, S., von Gunten, U., 2011. Efficiency and energy
573 requirements for the transformation of organic micropollutants by ozone, O_3/H_2O_2 and
574 UV/H_2O_2. Water Research 45 (13), 3811-3822.

575 Krämer, W., Schirmer, U., Jeschke, P., Witschel, M., 2008. Modern Crop Protection
576 Compounds, Volume 1: herbicides. Wiley-VCH Verlag GmbH & Co. KGaA

577 Kotoula-Syka, E., Eleftherohorino, I.G., Gagianas, A.A., Sficas, A.G., 1993.
578 Phytotoxicity and persistence of chlorsulfuron, metsulfuron-methyl, triasulfuron and
579 tribenuron-methyl in three soils. Weed Research 33 (5), 355-367.

580 Kowal, S., Balsaa, P., Werres, F., Schmidt, T.C., 2013. Fully automated standard
581 addition method for the quantification of 29 polar pesticide metabolites in different
582 water bodies using LC-MS/MS. Analytical and Bioanalytical Chemistry 405 (19), 6337-
583 6351.

584 Kuo, W.S., 1999. Synergistic effects of combination of photolysis and ozonation on
585 destruction of chlorophenols in water. Chemosphere 39 (11), 1853-1860.

586 Lam, M.W., Young, C.J., Mabury, S.A., 2005. Aqueous photochemical reaction kinetics
587 and transformations of fluoxetine. Environmental Science and technology 39 (2), 513-
588 522.

589 Márquez, G., Rodríguez, E.M., Beltrán, F.J., Álvarez, P.M., 2014. Solar photocatalytic
590 ozonation of a mixture of pharmaceutical compounds in water. Chemosphere 113, 71-
591 78.

592 Masschelein, W., Denis, M., Ledent, R., 1977. Spectrophotometric determination of
593 residual hydrogen peroxide. Water Sew Works 124(8), 69-72.

594 Mehrjouei, M., Müller, M., Möller, D., 2015. A review on photocatalytic ozonation
595 used for the treatment of water and wastewater. Chemical Engineering Journal 263 (1),
596 209-219.

597 Mena, E., Rey, A., Rodríguez, E.M., Beltrán, F.J., 2017. Nanostructured CeO2 as
598 catalysts for different AOPs based in the application of ozone and simulated solar
599 radiation. Catalysis Today 280 (1), 74-79.

600 Méndez-Arriaga, F., Otsu, T., Oyama, T., Giménez, J., Esplugas, S., Hidaka, H.,
601 Serpone, N., 2011. Photooxidation of the antidepressant drug Fluoxetine (Prozac®) in
602 aqueous media by hybrid catalytic/ozonation processes. Water Research 45 (9), 2782-
603 2794.

604 Menuer, L., Canonica, S.; von Gunten, U., 2006. Implications of sequential use of UV
605 and ozone for drinking water quality. Water Research 40 (9), 1864-1876.

606 Miklos, D.B., Remy, C., Jekel, M., Linden, K.G., Drewes, J.E., Hübner, U., 2010.
607 Evaluation of advanced oxidation processes for water and wastewater treatment. A
608 critical review. Water Research 139, 118-131.

Oh, J.S., Yajima, H., Hashida, K., Ono, T., Ishijima, T., Serizawa, I., Furuta, H., Hatta, A., (2016). In-situ UV absorption spectroscopy for observing dissolved ozone in water. Journal of Photopolymer Science and Technology 29 (3), 427-432.

Oturan, M.A., Aaron, J.J., 2014. Advanced oxidation processes in water/wastewater treatment: Principles and applications. A review. Critical Reviews in Environmental Science and Technology 44 (23), 2577-2641.

Parson, S., 2004. Advanced oxidation processes for water and wastewater treatment. IWA Publishing, London.

Pesticide Properties Database (PPDB), 2018. http://sitem.herts.ac.uk/aeru/ppdb/en/. Accessed 12 Jun 2018.

Poskrebyshev, G.A., Neta, P., Huie, R.E., 2002. Temperature dependence of the acid dissociation constant of the hydroxyl radical. The Journal of Physical Chemistry A 106, 11488-11491.

Quiñones, D.H., Álvarez, P.M., Rey, A., Beltrán, F.J., 2015. Removal of emerging contaminants from municipal WWTP secondary effluents by solar photocatalytic ozonation. A pilot-scale study. Separation and Purification Technology 149, 132-139.

Reemtsma, T., Alder, L., Banasiak, U., 2013. Emerging pesticide metabolites in groundwater and surface water as determined by the application of a multimethod for 150 pesticide metabolites. Water Research 47 (15), 5535-5545.

Rey, A., Quiñones, D.H., Álvarez, P.M., Beltrán, F.J., Plucinski, P.K., 2016. Simulated solar-light assisted photocatalytic ozonation of metoprolol over titania-coated magnetic activated carbon. Applied Catalysis B: Environmental 111-112, 246-253.

631 Rizzo, L., 2011. Bioassays as a tool for evaluating advanced oxidation processes in
632 water and wastewater treatment. Water Research 45 (15), 4311-4340.

633 Sarnah, A.K., Sabadie, J., 2002. Hydrolysis of sulfonylurea herbicides in soilds and
634 aqueous solutions: a review. Journal of Agricultural and Food Chemistry 50 (22), 6253-
635 6265.

636 Sauleda, R., Brillas, E., 2001. Mineralization of aniline and 4-chlorophenol in acidic
637 solution by ozonation catalyzed with Fe2+ and UVA light. Applied Catalysis B:
638 Environmental 29 (2), 135-145.

639 Serpone, N., Artemev, Y., Ryabchuk, V.K., Emeline, A.V., Horikoshi, S., 2017. Light-
640 driven advanced oxidation processes in the disposal of emerging pharmaceutical
641 contaminants in aqueous media. A brief review. Current Opinion in Green and
642 Sustainable Chemistry 6, 18-33.

643 Somathilake, P., Dominic, J.A., Achari, G., Langford, C.H., Tay, J.H., 2018.
644 Degradation of carbamazepine by photo-assisted ozonation: influence of wavelength
645 and intensity of radiation. Ozone: Science & Engineering 40 (2), 113-121.

646 Solís, R., Medina, S., Gimeno, O., Beltrán, F.J., 2019. Solar photolytic ozonation for the
647 removal of recalcitrant herbicides in river water. Separation & Purification Technology
648 212, 280-288.

649 Sousa, J.M.; Macedo G.; Pedrosa, M.; Becerra-Castro, C.; Castro-Silva, S.; Pereira,
650 F.R.; Silva, A.M.T.; Nunes, O.; Manaia, C.M., 2017. Ozonation and UV_{254} nm radiation
651 for the removal of microorganisms and antibiotic resistance genes from urban
652 wastewater. Journal of Hazardous Materials 323, 434-441.

Sthaehelin, J., Buhler, R.E., Hoigné, J., 1984 Ozone decomposition in water studied by pulse radiolysis.2. OH and HO4 as chain intermediates. Journal of Physical Chemistry 88 (24), 5999-6004.

Von Sonntag, C., von Gunten, U., 2012. Chemistry of ozone in water and wastewater treatment. IWA Publishing, London.

Zaltauskaité, J., Brazaityté, V., 2013. Assessment of the effects of sulfonylureas herbicide amidosulfuron application on target and non-target organisms. Fresenius Environmental Bulletin 22 (7), 1977-1982.

Xiao, J., Xie, Y., Cao, H., 2015. Organic pollutant removal in wastewater by heterogeneous photocatalytic ozonation. Chemosphere 121, 1-17.